Seeing the solvated electron in action: First-principles molecular dynamics of NO3– and N2O reduction

Jean Philippe Renault, Stanislas Pommeret

Seeing the solvated electron in action: first-principles molecular dynamics of NO_3^- and N_2O reduction

Jean Philippe Renault [a]*, and Stanislas Pommeret [b]

[a] *Université Paris-Saclay, CEA, CNRS, NIMBE, 91191, Gif-sur-Yvette, France*
[b] *Société Chimique de France, Paris, France*

[*] to whom correspondence should be addressed

Phone: (+33) 1 69 08 15 50

Email:jprenault@cea.fr

Abstract

Here, we studied the reactions of the solvated electron with nitrate or nitrous oxide using first-principles molecular dynamics simulations based on density-functional theory. We devised a strategy combining the *in situ* production of the aqueous electron followed by its reaction with either NO_3- or N_2O. The simulations revealed that electron transfer events occur on a sub-picosecond time scale and are controlled by the vibrational degree of freedom of the oxidants.

Keywords

Radiolysis, *ab initio* molecular dynamics, solvated electron, nitrate, N_2O, reduction

1. Introduction

Elementary radical reactions in liquid water are of primary importance for understanding chemical processes induced by ionising radiation, such as the production of hydrogen in nuclear waste storage (Rotureau et al. 2005) (Kaddissy et al. 2017) and radiobiology (Molin et al. 2007) (Le Goas et al. 2019), but also in a variety of processes as diverse as heterogeneous catalysis (Jaeger et al. 1979) and oxidative stress (Ohsawa et al. 2007). Although it is well known that elementary radical reactions are involved in all these processes, little is known about the details of the mechanisms involved, and especially the role of the solvent in these mechanisms..

Among radiolytic species, the solvated electron has been the most studied species since its discovery (Hart et al. 1962) 60 years ago. Its only reactivity is reductive, but its reduction rate can vary over five orders of magnitude. The explanation of this variability probably lies both in the structure of the reactants and in their solvation properties (Marcus 1965).

It may seem futile to try to write a reaction mechanism for a redox reaction, because it is usually viewed as a one-step process. Furthermore, the description of a mechanism for such a reaction is beyond the scope of the current electron transfer theories, which usually give a statistical description.

Nonetheless, here, our first objective was to determine the characteristic reaction times and determine which dynamic processes are associated with electron transfer in solvated electron reactions. First-principles molecular dynamics (FPMD) can be used to address this problem (Marsalek et al. 2012) through an explicit description of the electrons and the solvent. FPMD simulations based on density-functional theory (DFT) has been applied to the study of the solvation of radiolytic radicals in water (VandeVondele et al. 2005), or to the study of radical production in water during radiolytic processes (Gaigeot et al. 2007) (Renault et al. 2008). Interestingly, FPMD has been shown to provide a reliable description of the solvated electron (Boero et al. 2003, Prendergast et al. 2005, Boero 2007), (Turi et al. 2012), (Marsalek et al. 2012) and gives some insight as to its proton transfer and spectroscopic properties.

Other studies have addressed the question of electron “reactions” in water. However, these studies have all relied on vertical electron attachment, followed by its localisation/solvation (Smyth et al. 2011) (Liu et al. 2014) (Wu et al. 2015) (Dhungana et al. 2017), dissociative attachment of low energy electrons (Kohanoff et al. 2017) or even the reaction of sodium ion with a water cluster (Šmídová et al. 2015).

Our second objective was to reconcile the FPMD-DFT and electron localisation approaches to describe the reaction of a solvated electron after its stabilisation in water. More specifically, we studied the reaction mechanism for two prototypal aqueous electron reactions of crucial importance in the nuclear industry (Balcerzyk et al. 2012) (Gregson et al. 2018): the reduction of nitrate and the reduction of nitrous oxide.

The reduction of nitrate is a simple electron transfer leading to the formation of $NO_3^{2-\bullet}$, which has been observed both at low temperature by continuous irradiation (Lokkevik et al. 1969) and at room temperature by pulse radiolysis (Cook et al. 2001):

$$NO_3^- + e^- \rightarrow NO_3^{2-\bullet} \qquad \text{Eq. 1}$$

The reduction of nitrous oxide is a process that has been very well described in the gaseous phase in water clusters (Šmídová et al. 2015), and in a condensed (rare gas) phase. Two main mechanisms have been proposed:

$$N_2O + e^- \rightarrow N_2 + O^{\bullet-} \qquad \text{Eq. 2 (Nandi et al. 2014) and}$$

$$N_2O + e^- \rightarrow N_2O^- + M \rightarrow N_2 + O^{\bullet-} \qquad \text{Eq. 3 (Bartels et al. 1993).}$$

However, simulations tend to show that N_2O^- has a very short lifetime, from 30 fs (Suter et al. 2004) to 200-500 fs (Šmídová et al. 2015).

To analyse these two reduction reactions, we devised a strategy combining *in situ* production of the aqueous electron followed by its reaction either with NO_3^- or with N_2O.

2. Numerical methods

2.1. Generalities

Initial atomic configurations were obtained from classical molecular dynamics simulations (10 ns) employing an extended simple point-charge model (SPC/E) potential for water-water interactions (Berendsen et al. 1987). Constant-volume FPMD simulations in a spin-DFT framework were performed using the Born-Oppenheimer approximation with an integration time step of 0.1209 fs. The spin-dependent one-electron orbitals are expanded in a plane-waves basis set, with a kinetic energy cut-off of 70 Ry. The BLYP functional (Becke 1988) (Lee et al. 1988), which gives good results in liquid water (Sprik et al. 1996, Grossman et al. 2004). Standard norm-conserving, fully separable (Kleinman et al. 1982) *ab initio* pseudopotentials of the Troullier-Martins (Troullier et al. 1991) type were used for O and H. The simulations were conducted using the CPMD code (IBM 2004).

2.2. Self-interaction correction

The simulations took into account the so-called self-interaction correction (VandeVondele et al. 2005). The SSIC parameter of the simulation was set to 0.2. Higher values led to non-realistic behaviour of the solvated electron in the absence of reaction even after long simulation times. Lower values led to a delocalisation of the spin of the $HO^{\bullet}$ radical formed by reduction of N_2O.

Five simulations were conducted with 63 water molecules with one NO_3^- anion molecule and one distorted water molecule in a cube with periodic boundary conditions. Five simulations were also conducted with 63 water molecules with one N_2O molecule and one distorted water molecule. The box size was 12.71 Å for the nitrate simulations, and 12.57 Å for N_2O. No counter cations where introduced in the simulation, as FPMD allow to implicitly include in

simulations of non-neutral systems an homogeneous neutralizing background charge density without degrading the simulation performances (Todorova et al. 2008). The box was equilibrated for 1 ps using Car-Parrinello molecular dynamics (CPMD) before releasing the constraint and switching to Born-Oppenheimer molecular dynamics (BOMD). The temperature was set to 300 K and controlled using a Nosé-Hoover thermostat.
Figs. 2, 6 and 7 where prepared using VMD ((Humphrey et al. 1996). Classical molecular dynamics simulations where done using Moldy (Refson 2000).

3. Results

3.1. Production of the solvated electron

In the case of very reactive species such as N_2O and NO_3^-, reduction by solvated electrons cannot be achieved by simply adding an excess electron to the electronic structure (vertical reduction): this excess electron will naturally localise on the lowest unoccupied molecular orbit (LUMO) of the system during the wavefunction optimisation, which is mainly located on the solute. Therefore, we devised a method to control the localisation of the LUMO in the solvent by modifying defined atomic coordinates. The idea of this method was inspired by our study on the reaction between the hydroxide anion and the H atom (Renault et al. 2008). That study revealed that constraining a single HO bond of the solvent to more than 1.6 Å destabilised the corresponding MO sufficiently to induce the re-localisation of an excess electron on the H atom. Therefore, here, the first step of the reaction was an equilibration of the system with a distorted water molecule, i.e. with an elongated HO bond. This distortion was sufficient for i) localising the excess electron on the distorted water molecule during the initial optimisation of the wave function and ii) preventing its transfer to the solute during the equilibration process.

After releasing this constraint, the solvated electron formed in about 40 fs. These 40 fs can seem rather fast compared to the 240 fs measured by Gauduel, (Gauduel et al. 1989) but this short formation time indicates indeed a rather well preformed cavity around the elongated molecule during the equilibration step. CPMD failed to give an accurate description of electron behaviour in the water box after this time, probably because the coupling between the electronic degrees of freedom are not sufficiently connected with the nuclear degrees of freedom. Therefore, we used BOMD for this part of the simulation. The aqueous electron spectrum calculated using time-dependant DFT (Fig. S1, maximum at 1.4 eV and asymmetry toward the red end of the spectrum) showed a reasonable resemblance with the experimental spectrum (Jou et al. 1979), even though the calculated full width at half maximum (FWHM) was significantly lower, probably due to the duration of the simulation and box size effects.

3.2. Description of the reactions

3.2.1. Nitrous oxide

In all trajectories, the reductions of N_2O occurred within a picosecond and showed the same trends. We will here more extensively describe one of the trajectory in order to gain some insight for a proposal about the reaction mechanism

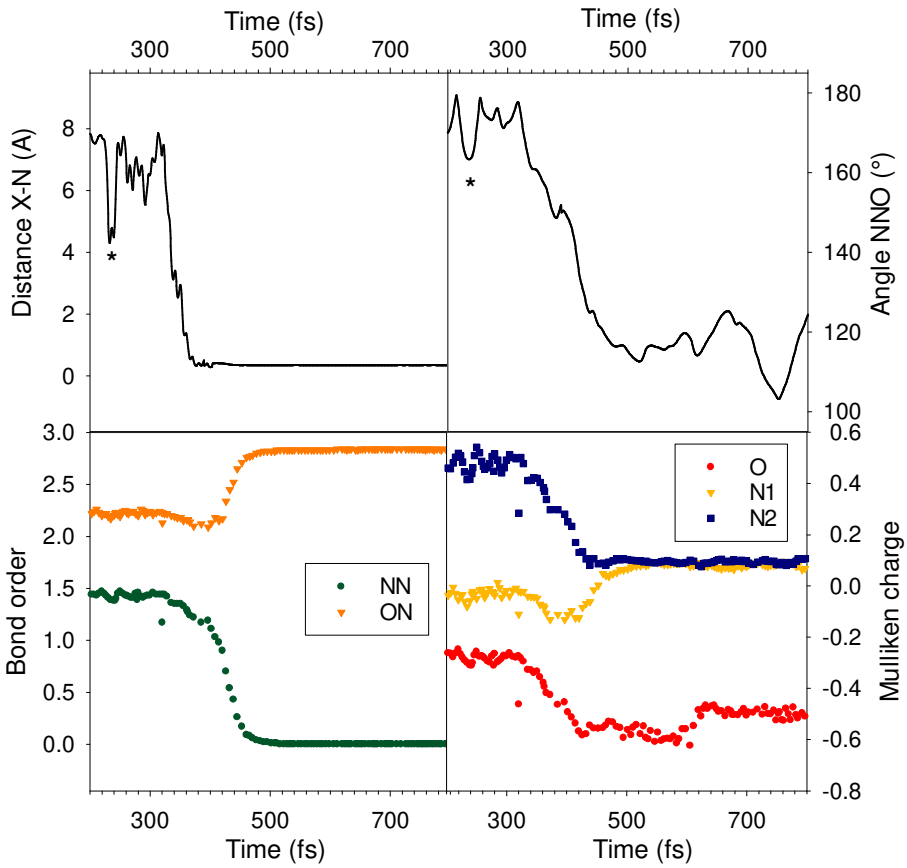

Fig. 1: Evolution of the most significant parameters during the reaction of the solvated electron with N_2O. X stands for the Wannier centre of the solvated electron. N2 is the central atom of N_2O.

For N_2O, two main steps can be distinguished in the reaction. The first step corresponds formally to the reduction observed through a brutal change in the distance between the Wannier centre of the electron and the central nitrogen atom of N_2O (X-N distance, Fig. 1). In the shown trajectory, this sudden drop in distance occurs 320 fs after electron production. The deformation of the N_2O molecule to accommodate the excess electron is concomitant to this transfer (Fig 1, NNO angle). This process is rapid (typically 40 fs) and occurs at distance of 6-8 Å between N_2O and the electron Wannier centre. These events can occur without the electron and N_2O sharing their solvation sphere, and, notably, aborted transfer can even be observed in some trajectories

(indicated by an asterisk in Fig. 1), both in the X-N distance and in the NNO angle. However, we can not affirm that these aborted events can explain the factor of four between the reaction kinetic and the Smoluchowski limit . (Takahashi et al. 2004)

It is known that electron attachment in the gas phase requires some activation energy to access — by vibrational excitation of the bending mode — the Franck–Condon transitions close to the crossing point between the neutral and anionic potential. The lowest crossing point between the energy curves of N_2O and the $N_2O^{-\bullet}$ anion occurs at a bond angle of about 30° (Takahashi et al. 2004), very similar to the angle at the end of the first reaction step observed here.

The definition of the end point for this first step is quite problematic, because the geometry of the reduction product is unstable and in constant evolution. However, we tentatively identified the formation of $N_2O^{-\bullet}$ at the pause in the bond order evolution between 380 and 410 fs (Fig. 1), which is also associated with a minimum Mulliken charge on the external nitrogen atom (Fig. 1). The lifetime of this state is comparable to the 30 fs simulated in the gas phase before dissociation.

This state keeps an NNO angle of 150±2°, and NO and NN bond lengths of respectively 1.28 and 1.16 Å. These values are significantly different from the optimised $N_2O^{-\bullet}$ anion either in vacuum or in a dielectric continuum, where the NNO angle is of about 130° (Suter et al. 2004). The reduction leads to a strongly distorted molecule whose geometry is far from equilibrated.

From a molecular orbital (MO) point of view, the electron is injected in one of the initially degenerated LUMOs with pi character in the oxide (Fig. 2 at 400 fs, Fig. S2).

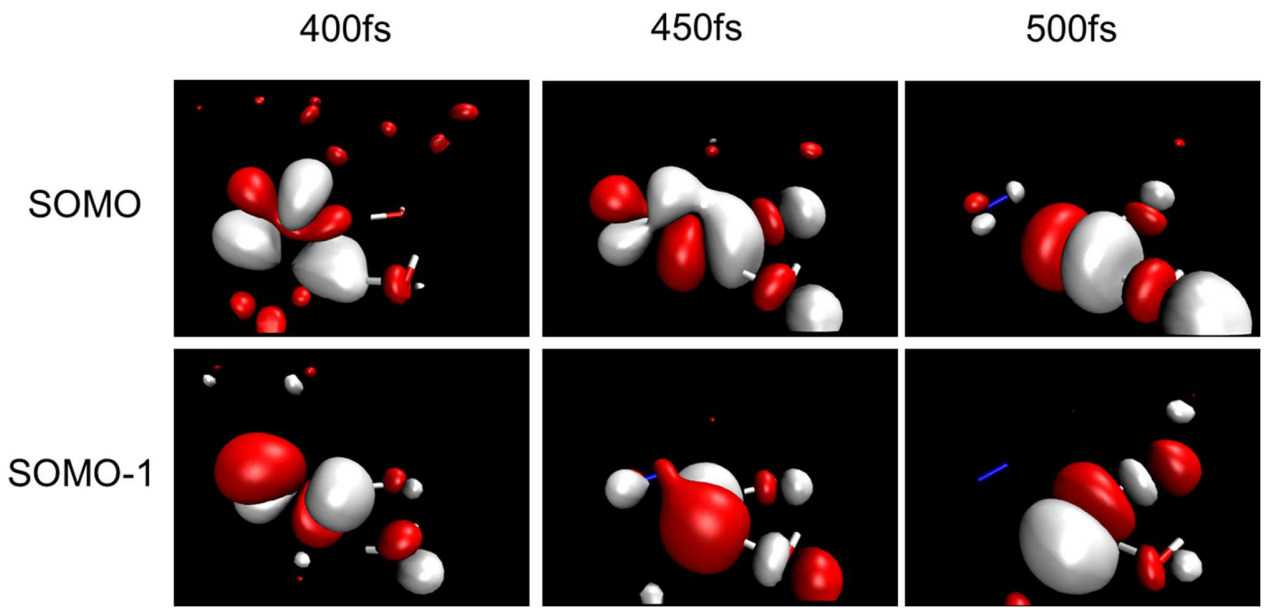

Fig. 2. Evolution of the shape of the singly occupied molecular orbital (SOMO), and of the doubly occupied molecular orbital nearest in energy, during the reduction of N_2O.

The electron transfer itself is connected to the appearance of orbital mixing between the LUMO of the N_2O and the singly occupied molecular orbital (SOMO) of the water cavity, apparent in their energetic quasi-degeneracy between 320 and 400 fs (indicated by an asterisk in Fig. S2). This mixing occurs through the networks of water antibonding orbitals, which constitute the lower part of the water conduction band (Fig. 2, scattered red spots). From an MO point a view, the "solvation" of an excess electron corresponds to its localisation in a MO formed by the overlap of OH antibonding orbitals (Renault et al. 2008) (Kumar et al. 2015).

The overall process is qualitatively different from the one proposed for the reaction between e^-_{aq} and CO_2. (Rybkin 2020) In this case, the reaction occurs only when CO_2 enters the solvated electron cavity and the $CO_2^{-\bullet}$ formation is reversible on a ps time scale.

In our case,he $N_2O^{-\bullet}$ anion has a limited lifetime of about 50 fs, significantly shorter than that observed in cluster dynamics (Šmídová et al. 2015). Its dissociation into N_2 and $O^{\bullet-}$, which is known in both the gas phase and in water, occurs between 420 and 480 fs. Breaking the NO bond requires a subtle reorganisation of the Wannier centres. The Wannier centres of oxygen are originally shifted towards nitrogen (a dative bond), giving bond orders higher than that of the NO bond (Fig. 1, Fig. 3A). The introduction of an additional electron favours bending due to pair repulsion and reduces the pi interaction (Fig. 3A-B), first between the N and the O and then between the two N atoms. As a result, bond order decreases both in the NO and the NN bonds (Fig. 1). The restoration of a high bond order for NN, energetically favourable (Fig. 3C), is concomitant to a disruption of the NO bond and to the acquisition of radical character by the oxygen (Fig 3D).

The rapid increase in the NO distance during the dissociation of the bond (Fig. 4) suggests that the NO interaction potential becomes repulsive. The N_2 moiety acquires significant kinetic energy, of about 0.5 eV (compared with 0.6 eV calculated in the gas phase (Suter et al. 2004)). There is no obvious residual vibrational excitation in N_2.

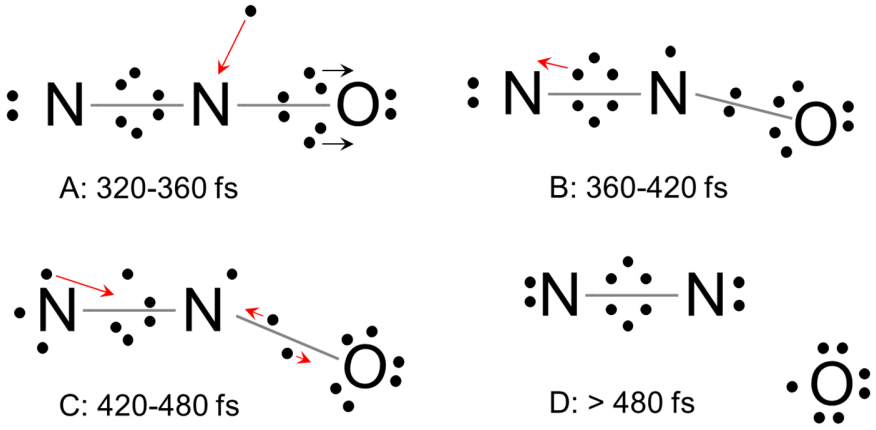

Fig. 3: Evolution of the Wannier centres during the various reduction steps.

Considering the evolution of the solvation environment during the first two steps, the major modification is the efficient recruitment (in less than 30 fs) of two neighbouring water molecules. Recruitment occurs by the creation of two hydrogen bonds with the oxygen atom of N_2O (one during the electron transfer itself, the second at the beginning of the NO dissociation) (Fig. 2 at 400 and 450 fs and Fig. 4).

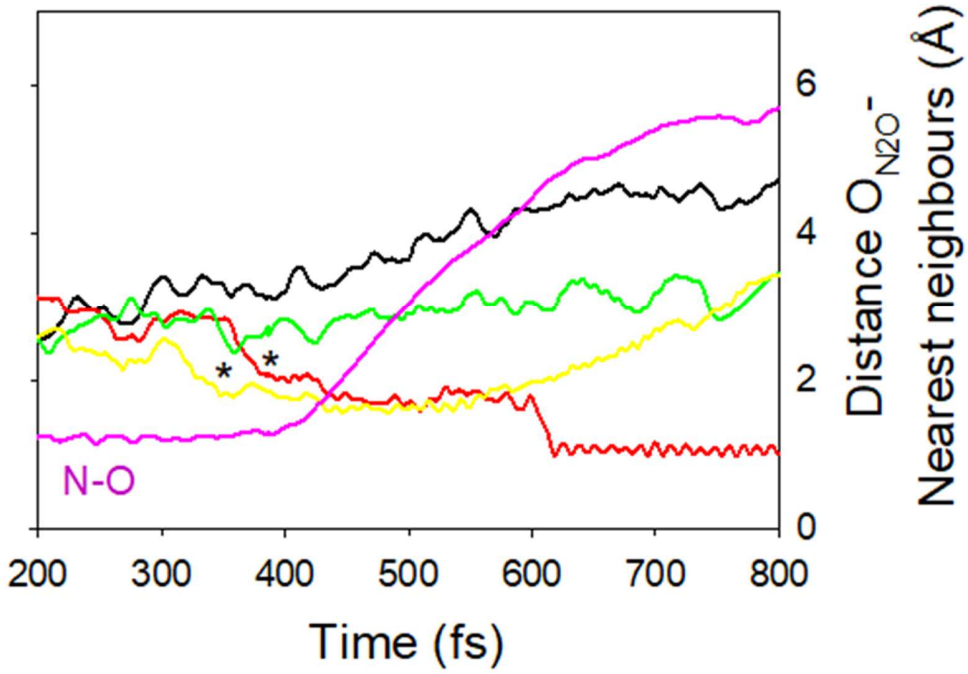

Fig. 4: Evolution of the environment around the oxygen atom of N_2O. All atoms are hydrogens of neighbouring water molecules, except for N (pink). The H bond formations are indicated by an asterisk.

From the Mulliken charges (Fig. 1), we can assume that the released oxygen remains $O^{\bullet-}$, but this atom remains strongly H-bonded to the two water molecules that have participated in the reaction ($O^{\bullet-}$-H distance of less than 2 Å). This $O^{\bullet-}$-$(H_2O)_2$ state lasts for about 100 fs (Fig. 2 at 500 fs). After this lapse of time, it abstracts a proton from one of the two participating water molecules, as already observed in water cluster simulations (Šmídová et al. 2015). The second water molecule is expelled with 0.14 eV of kinetic energy (Fig. 4), reminiscent of the quasi-hydrophobic nature of the HO radical (VandeVondele et al. 2005).

To summarise, the simulated process is very similar to the mechanism proposed in the gas phase, with a very transient formation of $N_2O^{-\bullet}$, and the emission of $O^{\bullet-}$ at significant velocity. Our observations therefore suggest a minimal role of the solvent in controlling the reaction after the reduction step.

3.2.2. Nitrate

As expected for a diffusion limited reaction, the reductions of NO_3^- occurs at the first encounter with the solvated electron in all simulated trajectories.

The main difference between N_2O and NO_3^- is the progressive nature of the NO_3^- reduction, which spans hundreds of fs. (Figs. 5 and 6)

From the change in the SOMO shape and the distances between the nitrogen and the Wannier centre of the unpaired electron (N-W distance in Fig. 5) in one representative trajectory, three main phases can be distinguished.

In the first phase, which lasts 150 fs, the distance between the nitrogen and the Wannier centre of the unpaired electron varies in a quasi-periodic fashion by up to 4 Å (Fig. 5). These variations correspond to a SOMO that changes periodically in character (Fig. 6), being either mainly centred on the initial electron (long N-W distances), solvation cavity or on the nitrate solvation cavity (short N-W distances). These oscillations are not associated with increased electron localisation, as shown by the Wannier spread (Fig. 5). We also noted the particular role of the water molecule, which seems to provide an orbital connection between the two cavities. Donor-acceptor coupling through solvent has indeed been recently emphasised in small molecular systems (Troisi et al. 2004) (Skourtis et al. 2010).

In the second phase, after 150 fs, the SOMO is formed by the overlap of NO_3^- antibonding pi orbitals and of the nearby water molecule (Fig. 6). The Wannier centre of the unpaired electron

is also not centred on the nitrogen, but spreads over the whole water cavity (data not shown) surrounding the nitrate. This part of the reaction is strongly reminiscent of a charge-transfer-to-solvent (CTTS) state (Kunin et al. 2019).

In the third phase, during the last 50 fs, the electron relocalises from the solvent cavity onto the nitrogen itself. This event is associated with a significant gain in energy of the SOMO (Fig. 5). At the end of the reaction, the unpaired electron is in a non-bonding orbital centred on the nitrogen, forming the expected $NO_3^{2-\bullet}$. During the whole process, the Mulliken charges on the nitrate decrease progressively (Fig. S5). The obtained structure of the dianion (ONO angle of 113° and NO length of 1.32 Å) is comparable to that obtained in a vacuum at the MP2(full)/6-31G* level (ONO angle of 116° and NO length of 1.36 Å) (Cook et al. 2001), but is not perfectly symmetric.

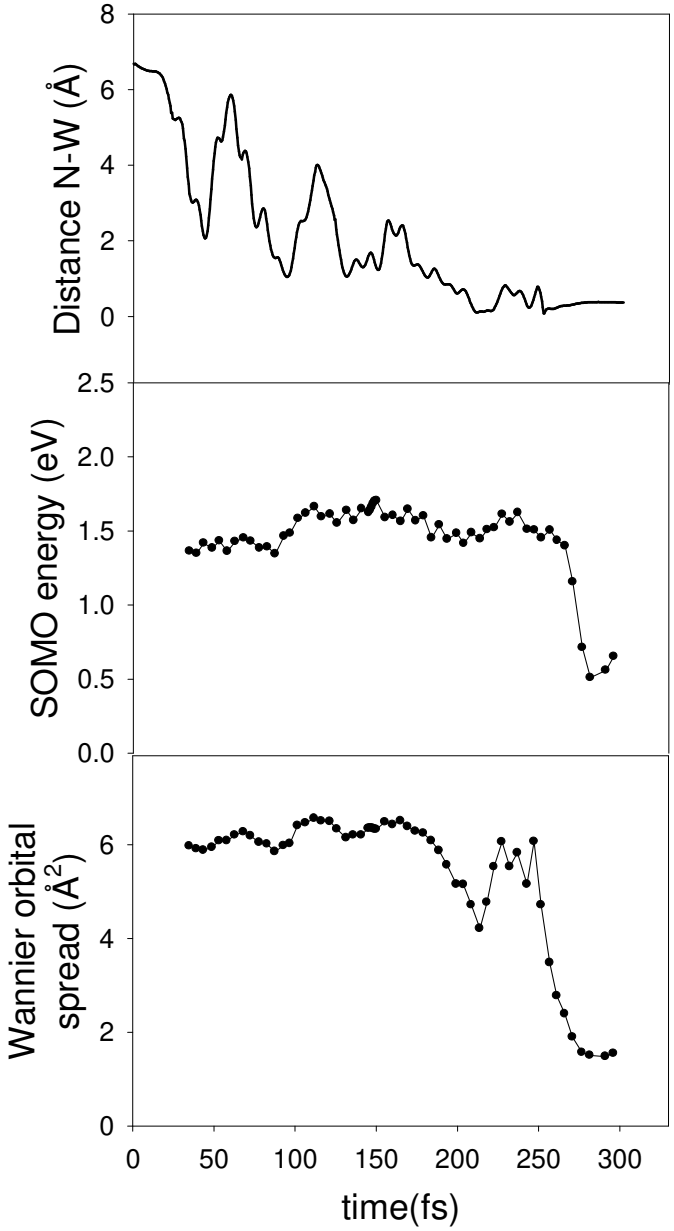

Fig. 5: Evolution of the significant parameters during the reaction of the solvated electron with NO_3^-.

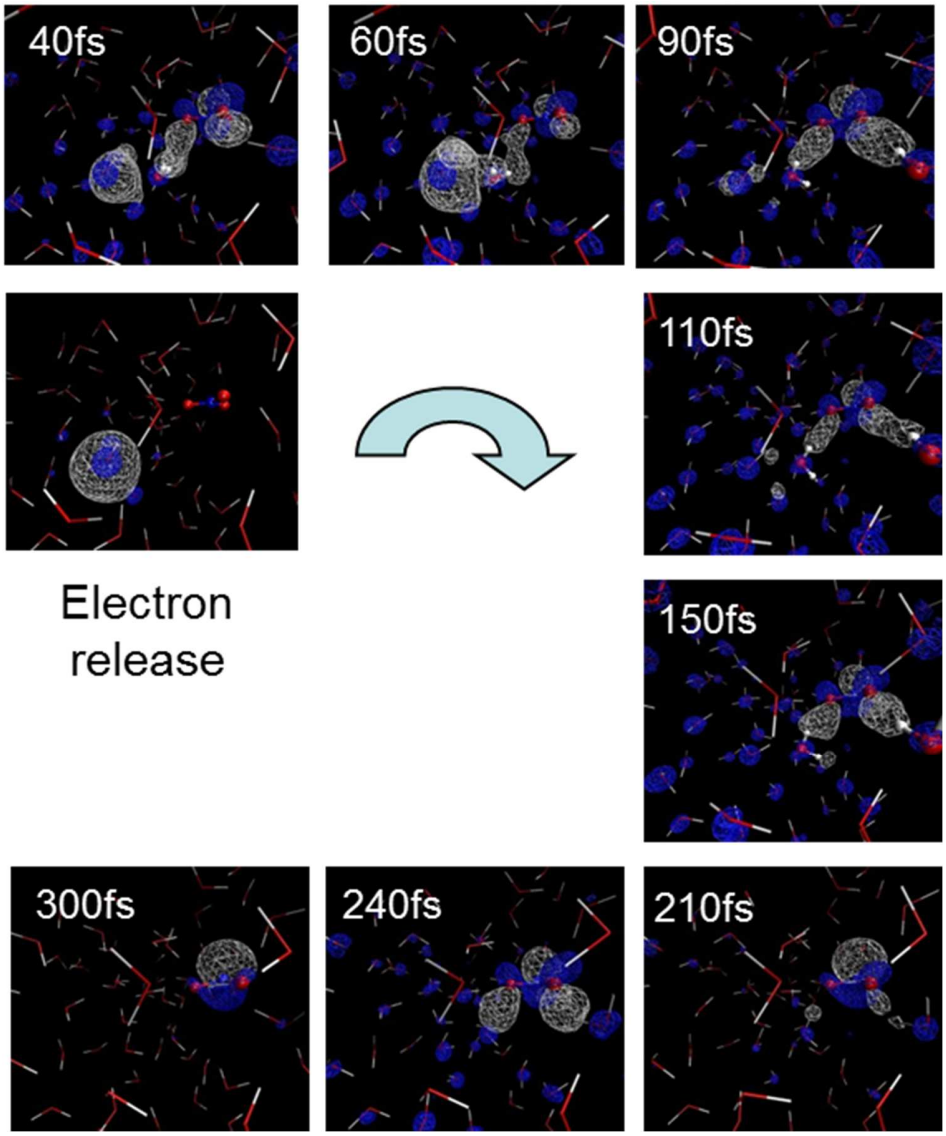

Fig 6. Evolution of the shape of the singly occupied molecular orbital (SOMO) during nitrate reduction.

Two questions arise:

-what force drives the oscillations?

-what is the source of irreversibility of the process?

We were able to identify the source of the oscillation with the umbrella mode of NO_3^-, (the so-called υ_2 mode, see Fig. S4). We suggest that this deformation drives the orbital interaction between the initial water cavity and the solvated nitrate, by transiently stabilising the NO_3^- antibonding orbitals where the electron will ultimately relocalise. It can indeed be defined as the

reaction coordinate.

For the source of irreversibility, we can exclude a significant energetic gain, because the SOMO stabilises only at the end of the process (see the SOMO energy in Fig. 5). Instead, we suggest that the initial water cavity progressively disappears during its back-and-forth movements corresponding to vibrational motions of the water forming the solvated electron cavity. This disappearance is concordant with the progressive charge transfer towards the nitrate, revealed by the decrease in Mulliken charges. From Fig. S5, the trend is clear, with a charge transfer that affects the $O_{nitrate}$ throughout the entire reaction. This increase in charge around the nitrate is obviously the signature of a progressive decrease of the charge in water, which can only lead to the disappearance of the water cavity. In addition, this progressive charge transfer is associated with a progressive damping/distortion of the nitrate umbrella motions to accommodate this excess charge.

The reorganisation of the solvent around the nitrate occurs after the electron transfer. Three to four solvating water molecules stand initially in the nitrate plane, as expected from the hydrogen interaction with the non-bonding pair located on the nitrate oxygen atoms in the Lewis representation. The in-plane position of this pair is obvious from the electron localisation function (ELF) representation and corresponds to the SP_2 hybridisation of these sites (Fig. S6)

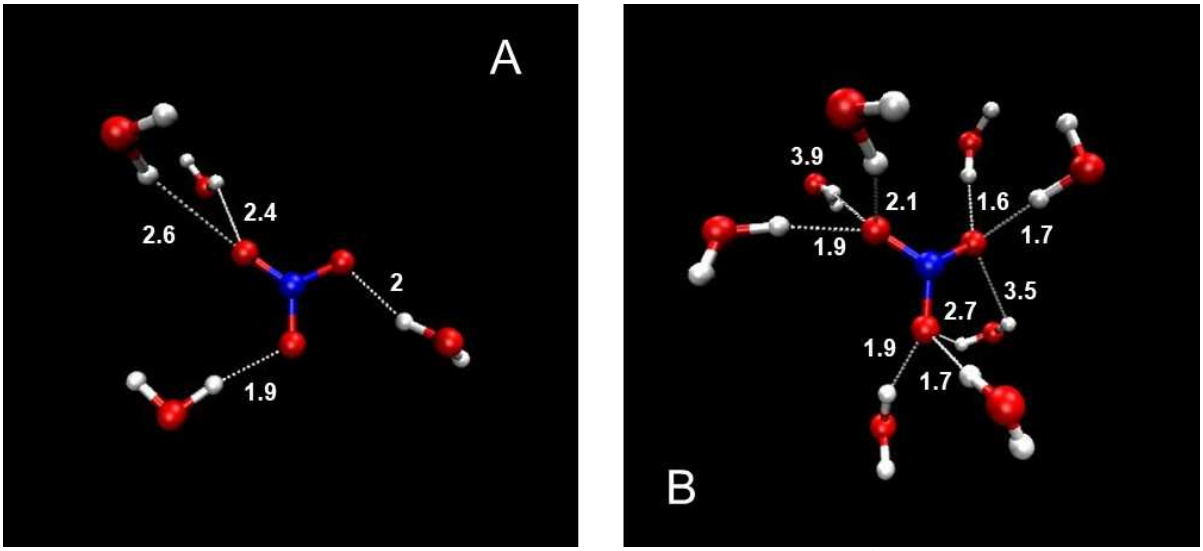

Fig. 7A) Solvation around NO_3^- (t = 0 fs), B) Solvation around $NO_3^{2-\bullet}$. Distances are given in Angstroms (Å).

The $NO_3^{2-\bullet}$ final state is solvated by five to seven water molecules in pseudo-tetrahedral arrangements. These arrangements can be explained by the doughnut shape of the non-bonding pairs (Fig. S6). The $O_{nitrate}$-H_{water} distances are notably shorter than for aqueous nitrate,

demonstrating that $NO_3^{2-\bullet}$ develops a stronger interaction with water than does $NO_3^{-\cdot}$

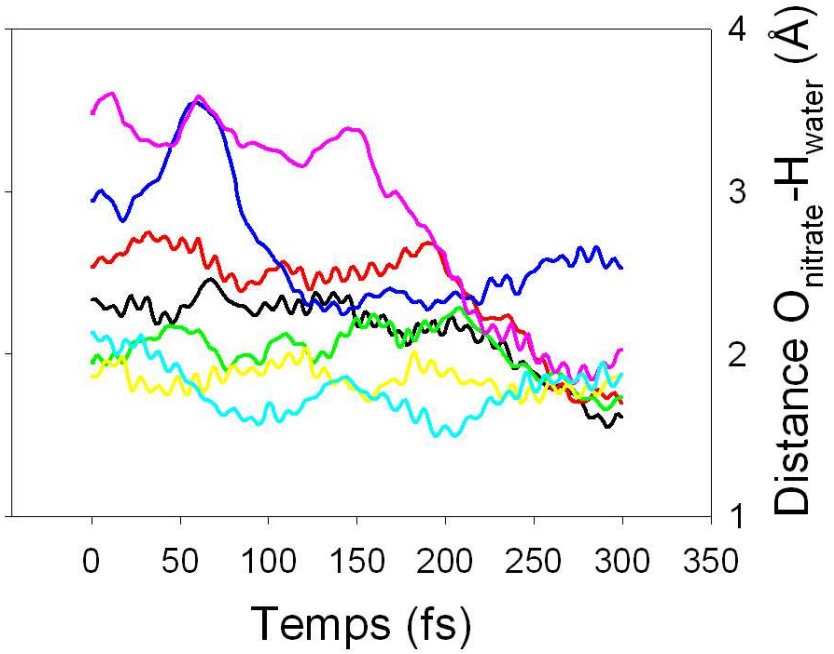

Fig. 8: Evolution of the environment around the oxygen atom of NO_3^-.

Between these two solvation states, there is obviously a strong reorganisation of the solvent sphere associated with the electron transfer upon the recruitment of two to three H_2O molecules after 150 fs (i.e. after the electron has localised on the nitrate solvation cage). A typical change in the $O_{nitrate}$-H_{water} distance as a function of time is shown in Fig. 8. The recruitment takes longer than in the N_2O case, from 100 to 150 fs, suggesting that the solvent around NO_3^- is less mobile than around N_2O.

4. Discussion

The reactions we looked at are diffusion or near diffusion limited in solution. (For N_2O, the reaction is only a factor of four below the Smoluchowski limit (Takahashi, et al 2004). Therefore, the various theories of electron transfer may seem irrelevant at first. However, the reaction mechanisms and behaviour we observed are sufficiently diverse to suggest fundamental differences in the underlying energetics between NO_3^- and N_2O, which we endeavour to analyse here in the light of these theories. Several dependencies have been proposed for electron transfer processes in various theoretical models (Landau-Zener, Marcus, Levich-Dogonadze) or more generally in reaction rate theories (Lindemann-Hinshelwood, Kramers).For exemple the Marcus theory express the electron transfer rate as (Marcus 1993)

$$k_{electron-transfer} = \frac{2\pi}{\hbar} \frac{|H_{AB}|^2}{\sqrt{4\pi\lambda k_b T}} \exp\left(-\frac{(\lambda+\Delta G_0)^2}{4\lambda k_b T}\right) \qquad \text{Eq. 4}$$

Where (H_{AB}) is electronic coupling between the initial and final states, ΔG_0 is the variation in free enthalpy, and λ and the reorganisation energy (internal and solvent related) associated to the reaction.

4.1. The role of electronic coupling (H_{AB})

A distinction is currently made between adiabatic electron transfers, where the H_{AB} electronic coupling is strong, and nonadiabatic transfers, where this coupling is more limited. In adiabatic processes, electron transfer is fast compared with the change in the nuclear configuration, whereas in non-adiabatic processes, the vibrational motions are faster than the charge redistribution/electron transfer.

First, from a purely quantum mechanical view, the simulations that we conducted within the Born-Oppenheimer approximation remain adiabatic . However, for the fast electron transfer considered here, electron transfers should be discussed as the temporal evolution of the electronic probability density from one site to another, which we monitored in this study using Wannier localisation. Thus, locally adiabatic or locally diabatic processes are considered with respect to this Wannier centre.

The electron transfer to NO_3^- can be described as slow. It is clearly locally adiabatic, because it follows a defined (vibrational) reaction coordinate. It is indeed strongly reminiscent of experiments conducted on ultrafast wave packet dynamics (Kambhampati et al. 2000).

On an fs time scale, the electron transfer to N_2O shows the same adiabatic behaviour, because it is connected to the NNO bending. However, when put in the context of a longer time scale (a few fs), the electron transfer clearly resembles a diabatic process, where a masked, solvent-connected reaction coordinate triggers the electron transfer. The aborted transfer events in Fig. 1 are a clear proof of the existence of such a hidden coordinate. We were not able to identify this coordinate unambiguously, even though the solvent may play a role in opening an electronic coupling channel (through water H-bonds) between the solvated electron cavity and N_2O. Here, we encountered a phenomenon that is more usually analysed in biological electron transfers, where the electron transfer depends on the fluctuations of a tunnelling bridge/pathway between the donor and acceptor.

To confirm these differences in electronic coupling between N_2O and NO_3^-, we studied the energy fluctuations of the frontier orbital involved in the electron transfer. We considered that the magnitude of the fluctuations reflect the slope of the potential energy surface with respect to a nuclear coordinate, and thus one-eighth of the potential barrier to be crossed.

For NO_3^-, the energies of the SOMO and of the SOMO+1 are almost degenerate and show minimal fluctuations (Fig. S3), suggesting a very small barrier, compatible with a local

adiabadicity. For N_2O in water, the SOMO (the solvated electron) and the SOMO+1 as well as SOMO+2 (that we can call, from their localisation, the LUMO of N_2O) first seem non-correlated, with strong fluctuations of the LUMOs, due to NNO bending. The advent of stronger coupling between the SOMO and one of the LUMOs is concomitant with the electron transfer process itself.

4.2. Variation in free enthalpy (ΔG)

For the nitrate reduction by solvated electron, a ΔG value of -78 kJ/mol has been suggested. (Cook et al. 2001) to be compared with a ΔG value of -137 kJ/mol for N_2O reduction (Takahashi et al. 2004). Such high values suggest the possibility of a reaction occurring within the so-called Marcus inverted region, thus decreasing the probability of electron transfer (Ichino et al. 2007). In these conditions, electron transfer can only occur in a configuration requiring high reorganisation energy We did not observe any indication of such stringent conditions for electron transfer.

4.3. Reorganisation energy (solvent friction)

For ultrafast electron transfer reactions, the dynamical effects involving nuclear motions of the reactants and the solvent are often mentioned as the key determinants. However, most studies have been looking for a solvent control through its inertial component. Our observation emphasises that internal reorganisation is the major reaction coordinate for both N_2O and NO_3^-
This is a typical configuration described by Hupp et al. (Hupp et al. 2001) in which a vibrational barrier connected to structural differences between reactants and products defines the dynamics of the overall reaction. This configuration occurs “when solvation contributes comparatively little to the activation barrier, and if electronic communication is good”. Crossing this barrier for low-frequency modes requires classical thermal activation (Hupp et al. 2001) (Abraham et al. 2019). In particular, under vibrational control, the reaction is not expected to slow down in the Marcus inverted region (Hupp et al. 2001).
This vibrational barrier can be calculated using Eq. 2:

$$\lambda_{vib} = 0.5\sum \Delta_k^2 \upsilon_k \quad , \qquad \text{Eq. 5}$$

where Δ is the bond length/angle change in the various normal modes and υ, the force constant associated with this mode. The analysis is quite simple here, because for both NO_3^- and N_2O, a single mode is involved.
For N_2O, the bending variation is 20° for the initial electron transfer, with an associated reorganisation energy that is comparatively smaller, about 14 kJ/mol (using the force constant tabulated by Hertzberg). (Herzberg 1945) This value is comparable to the activation energies of the reactions. For NO_3^-, the average improper angle around the nitrogen increases by 20° at the end of the reaction. The associated reorganisation energy can be evaluated at from 40 kJ/mol (Vchirawongkwin et al.) to 80 kJ/mol (Herzberg 1945). This value is large compared with the activation energies found in the literature (i.e. less than 20 kJ/mol). However, the disappearance

of the solvated electron (observable during experiments) requires only a variation of 10°, with an activation energy in agreement with the literature data.
Now, we can consider solvent reorganisation (also called solvent friction), which occupies a prominent role in electron transfer theory.

Electron transfer rates often appear connected to the dielectric relaxation properties of the solvent (Rafiq et al. 2019). This solvent effect is usually explained through an electrostatic levelling of the reactant and product energy: the electron transfer occurs when the solvent adopts a configuration electrostatically favourable to the product state. We indeed observed solvent reorganisation, but only after the initiation of the charge transfer. For the reactions studied here, solvent reorganisation does not control the electron transfer, but stabilises the reduced state configuration. The electron transfer process is indeed faster than the water translational dynamics, which can be characterised by a solvation time of 100 fs for NO_3- and of 50 fs for N_2O (Figs. 4 and 8).

For NO_3-, solvent reorganisation also controls the escape of the Franck–Condon region for allowed electron transfer through the collapse of the electron solvation cavity. Our simulations give an upper time limit for this process of 150 fs. It is thus tempting to compare this value as a reference time for the formation of a cavity around an electron, the so called solvation process, which has a characteristic time of 100 to 250 fs in water (Gauduel et al. 1989, Turi et al. 2012)(Pizzochero et al. 2019). These changes (loss of the electron cavity, stronger solvation around $NO_3^{2-\bullet}$) can explain the high negative entropy of activation of the reaction, interpreted as electrostriction (Lai et al. 1990). At this point, the solvents' dielectric properties are notably also connected to their internal structural fluctuations. Therefore, the dependence of electron transfer on solvent dielectric properties may also reflect the role of solvent reorganisation in controlling other critical electron transfer parameters, such as exchange integrals.

4.4 Solvated electron behaviour

The reactivity of the solvated electron is thus connected to the solvent properties, which control the electronic coupling with the scavengers like a bridge in donor-acceptor systems (Troisi et al. 2004), and to the scavengers' internal dynamics themselves. Therefore, a good way to describe the electron transfer behaviour of the solvated electron is to use the concepts developed for intramolecular electron transfer.
The extensively solvated NO_3^- presents strong coupling with the solvated electron and allows a reaction that is reminiscent of a superexchange, whereas the less coupled N_2O follows a hopping-like transport mechanism (Okada et al. 1998). Furthermore, the oscillatory behaviour of nitrate seems to correspond well to that observed in many ultrafast experiments (Abraham et al. 2019) (Ampadu Boateng et al. 2019).
We also note that we never needed to call upon the concept of electrostatic repulsion between the reactants. At the nanometric scale considered, the charges of both the electron and of the nitrate

anion are both highly distributed. This phenomenon is well known from experiments at low temperature (Marshall et al. 1975) and can be explained by the delocalised nature of the solvated electron that spreads the charge around its water cavity. However, at a larger scale, during the formation of the reactive complex, this effect cannot be ignored and is indeed the basis of the identification of the reducing species in radiolysis as a solvated electron. (Czapski et al. 1962).

5. Conclusions

The aqueous electron transfer process can be described with a low number of relevant processes, the major one being the reactant vibrational reorganisation and electronic interactions mediated by the solvent. Furthermore, our results suggest the more extensive use of combined pulsed radiolysis/photochemical experiments to analyse electron reactivity further, e.g. for studying UV visible photoexcitation of the $NO_3^{2-\bullet}$ state, to try to observe loosely bound CTTS states or the effect of specific mode activation, by infrared photolysis, on electron transfer.

6. **References**.

Abraham, B., L. G. C. Rego and L. Gundlach (2019). "Electronic–Vibrational Coupling and Electron Transfer." The Journal of Physical Chemistry C **123**(39): 23760-23772.
Ampadu Boateng, D., M. K. D. Word, L. G. Gutsev, P. Jena and K. M. Tibbetts (2019). "Conserved Vibrational Coherence in the Ultrafast Rearrangement of 2-Nitrotoluene Radical Cation." The Journal of Physical Chemistry A **123**(6): 1140-1152.
Balcerzyk, A., A. K. El Omar, U. Schmidhammer, P. Pernot and M. Mostafavi (2012). "Picosecond Pulse Radiolysis Study of Highly Concentrated Nitric Acid Solutions: Formation Mechanism of NO3• Radical." The Journal of Physical Chemistry A **116**(27): 7302-7307.
Bartels, D. M. and S. P. Mezyk (1993). "Epr Measurement of the Reaction of Atomic-Hydrogen with Br- and I- in Aqueous-Solution." Journal of Physical Chemistry **97**(16): 4101-4105.
Becke, A. D. (1988). "Density-functional exchange-energy approximation with correct asymptotic behavior." Physical Review A **38**(6): 3098 LP - 3100.
Berendsen, H. J. C., J. R. Grigera and T. P. Straatsma (1987). "The missing term in effective pair potentials." J. Phys. Chem. **91**(24): 6269-6271.
Boero, M. (2007). "Excess Electron in Water at Different Thermodynamic Conditions." J. Phys. Chem. A **111**(49): 12248-12256.
Boero, M., M. Parrinello, K. Terakura, T. Ikeshoji and C. C. Liew (2003). "First-principles molecular-dynamics simulations of a hydrated electron in normal and supercritical water." Physical Review Letters **90**(22).
Cook, A. R., N. Dimitrijevic, B. W. Dreyfus, D. Meisel, L. A. Curtiss and D. M. Camaioni (2001). "Reducing Radicals in Nitrate Solutions. The NO32- System Revisited." The Journal of Physical Chemistry A **105**(14): 3658-3666.
Czapski, G. and H. A. Schwarz (1962). "THE NATURE OF THE REDUCING RADICAL IN WATER RADIOLYSIS 1." The Journal of Physical Chemistry **66**(3): 471-474.
Dhungana, K. B., F. Wu and C. J. Margulis (2017). "Excess Electron and Hole in 1-Benzylpyridinium-Based Ionic Liquids." Journal of Physical Chemistry B **121**(37): 8809-8816.
Gaigeot, M. P., R. Vuilleumier, C. Stia, M. E. Galassi, R. Rivarola, B. Gervais and M. F. Politis (2007). "A multi-scale ab initio theoretical study of the production of free radicals in swift ion tracks in liquid water." Journal of Physics B-Atomic Molecular and Optical Physics **40**(1): 1-12.
Gauduel, Y., S. Pommeret, A. Migus and A. Antonetti (1989). "Femtosecond dynamics of geminate pair recombination in pure liquid water." The Journal of Physical Chemistry **93**(10): 3880-3882.
Gregson, C. R., G. P. Horne, R. M. Orr, S. M. Pimblott, H. E. Sims, R. J. Taylor and K. J. Webb (2018). "Molecular Hydrogen Yields from the α-Self-Radiolysis of Nitric Acid Solutions Containing Plutonium or Americium." The Journal of Physical Chemistry B **122**(9): 2627-2634.
Grossman, J. C., E. Schwegler, E. W. Draeger, F. Gygi and G. Galli (2004). "Towards an assessment of the accuracy of density functional theory for first principles simulations of water." Journal of Chemical Physics **120**(1): 300-311.

Hart, E. J. and J. W. Boag (1962). "Absorption Spectrum of the Hydrated Electron in Water and in Aqueous Solutions." Journal of the American Chemical Society **84**(21): 4090-4095.
Herzberg, G. (1945). Infrared and raman spectra of polyatomic molecules. Princeton, Van Nostrand.
Humphrey, W., A. Dalke and K. Schulten (1996). "VMD: Visual molecular dynamics." Journal of Molecular Graphics **14**(1): 33-&.
Hupp, J. T. and R. D. Williams (2001). "Using Resonance Raman Spectroscopy To Examine Vibrational Barriers to Electron Transfer and Electronic Delocalization." Accounts of Chemical Research **34**(10): 808-817.
IBM (2004). "CPMD." version 3.9.1; Festkorperforschung Stuttgart and IBM Zurich Research Laboratory, 2004 (http://www.cpmd.org).
Ichino, T. and R. W. Fessenden (2007). "Reactions of Hydrated Electron with Various Radicals: Spin Factor in Diffusion-Controlled Reactions." The Journal of Physical Chemistry A **111**(13): 2527-2541.
Jaeger, C. D. and A. J. Bard (1979). "Spin Trapping and Electron-Spin Resonance Detection of Radical Intermediates in the Photo-Decomposition of Water at Tio2 Particulate Systems." Journal of Physical Chemistry **83**(24): 3146-3152.
Jou, F.-Y. and G. R. Freeman (1979). "Temperature and isotope effects on the shape of the optical absorption spectrum of solvated electrons in water." The Journal of Physical Chemistry **83**(18): 2383-2387.
Kaddissy, J. A., S. Esnouf, D. Durand, D. Saffre, E. Foy and J.-P. Renault (2017). "Radiolytic Events in Nanostructured Aluminum Hydroxides." The Journal of Physical Chemistry C **121**(11): 6365-6373.
Kambhampati, P., D. H. Son, T. W. Kee and P. F. Barbara (2000). "Solvent Effects on Vibrational Coherence and Ultrafast Reaction Dynamics in the Multicolor Pump−Probe Spectroscopy of Intervalence Electron Transfer." The Journal of Physical Chemistry A **104**(46): 10637-10644.
Kleinman, L. and D. M. Bylander (1982). "Efficacious Form for Model Pseudopotentials." Physical Review Letters **48**(20): 1425 LP - 1428.
Kohanoff, J., M. McAllister, G. A. Tribello and B. Gu (2017). "Interactions between low energy electrons and DNA: a perspective from first-principles simulations." Journal of Physics-Condensed Matter **29**(38).
Kumar, A., J. A. Walker, D. M. Bartels and M. D. Sevilla (2015). "A Simple ab Initio Model for the Hydrated Electron That Matches Experiment." The Journal of Physical Chemistry A **119**(34): 9148-9159.
Kunin, A. and D. M. Neumark (2019). Femtosecond Time-Resolved Photoelectron Spectroscopy of Molecular Anions. Physical Chemistry of Cold Gas-Phase Functional Molecules and Clusters. T. Ebata and M. Fujii. Singapore, Springer Singapore**:** 307-335.
Lai, C. C. and G. R. Freeman (1990). "Solvent effects on the reactivity of solvated electrons with charged solutes in methanol/water and ethanol/water mixed solvents." The Journal of Physical Chemistry **94**(12): 4891-4896.
Le Goas, M., A. Paquirissamy, D. Gargouri, G. Fadda, F. Testard, C. Aymes-Chodur, E. Jubeli, T. Pourcher, B. Cambien, S. Palacin, J.-P. Renault and G. Carrot (2019).

"Irradiation Effects on Polymer-Grafted Gold Nanoparticles for Cancer Therapy." ACS Applied Bio Materials **2**(1): 144-154.
Lee, C., W. Yang and R. G. Parr (1988). "Development of the Colle-Salvetti correlation-energy formula into a functional of the electron density." Physical Review B **37**(2): 785 LP - 789.
Liu, J., R. I. Cukier, Y. Bu and Y. Shang (2014). "Glucose-Promoted Localization Dynamics of Excess Electrons in Aqueous Glucose Solution Revealed by Ab Initio Molecular Dynamics Simulation." Journal of Chemical Theory and Computation **10**(10): 4189-4197.
Lokkevik, P. and Henrikse.T (1969). "RADIATION-INDUCED FREE RADICALS IN FROZEN NITRIC ACID SOLUTIONS." Radiation Research **38**(2): 231-&.
Marcus, R. A. (1965). "Theory of Electron-Transfer Reaction Rates of Solvated Electrons." The Journal of Chemical Physics **43**(10): 3477-3489.
Marcus, R. A. (1993). "Electron Transfer Reactions in Chemistry: Theory and Experiment (Nobel Lecture)." Angewandte Chemie International Edition in English **32**(8): 1111-1121.
Marsalek, O., F. Uhlig, J. VandeVondele and P. Jungwirth (2012). "Structure, Dynamics, and Reactivity of Hydrated Electrons by Ab Initio Molecular Dynamics." Accounts of Chemical Research **45**(1): 23-32.
Marshall, E. J., M. J. Pilling and S. A. Rice (1975). "Electron tunnelling in glassy media. γ-Radiolysis investigation of electron scavenging in methanol, 2-methyltetrahydrofuran and 10 mol dm–3 hydroxide glasses at 77 K." Journal of the Chemical Society, Faraday Transactions 2: Molecular and Chemical Physics **71**(0): 1555-1562.
Molin, M., J.-P. Renault, G. Lagniel, S. Pin, M. Toledano and J. Labarre (2007). "Ionizing radiation induces a Yap1-dependent peroxide stress response in yeast." Free Radical Biology and Medicine **43**(1): 136-144.
Nandi, D., V. S. Prabhudesai and E. Krishnakumar (2014). "Dissociative electron attachment to N2O using velocity slice imaging." Physical Chemistry Chemical Physics **16**(9): 3955-3963.
NDRL. (2002). "NDRL/NIST Solution Kinetics Database on the Web, A compilation of kinetics data on solution-phase reactions." 2020.
Ohsawa, I., M. Ishikawa, K. Takahashi, M. Watanabe, K. Nishimaki, K. Yamagata, K.-i. Katsura, Y. Katayama, S. Asoh and S. Ohta (2007). "Hydrogen acts as a therapeutic antioxidant by selectively reducing cytotoxic oxygen radicals." **13**(6): 688-694.
Okada, A., V. Chernyak and S. Mukamel (1998). "Solvent Reorganization in Long-Range Electron Transfer: Density Matrix Approach." The Journal of Physical Chemistry A **102**(8): 1241-1251.
Pizzochero, M., F. Ambrosio and A. Pasquarello (2019). "Picture of the wet electron: a localized transient state in liquid water." Chemical Science **10**(31): 7442-7448.
Prendergast, D., J. C. Grossman and G. Galli (2005). "The electronic structure of liquid water within density-functional theory." Journal of Chemical Physics **123**(1).
Rafiq, S. and G. D. Scholes (2019). "From Fundamental Theories to Quantum Coherences in Electron Transfer." Journal of the American Chemical Society **141**(2): 708-722.
Refson, K. (2000). "Moldy: a portable molecular dynamics simulation program for serial and parallel computers." Computer Physics Communications **126**(3): 310-329.

Renault, J. P., R. Vuilleumier and S. Pommeret (2008). "Hydrated Electron Production by Reaction of Hydrogen Atoms with Hydroxide Ions: A First-Principles Molecular Dynamics Study." The Journal of Physical Chemistry A **112**(30): 7027-7034.
Rotureau, P., J. P. Renault, B. Lebeau, J. Patarin and J. C. Mialocq (2005). "Radiolysis of Confined Water: Molecular Hydrogen Formation." Chemphyschem **6**(7): 1316-1323.
Rybkin, V. V. (2020). "Mechanism of Aqueous Carbon Dioxide Reduction by the Solvated Electron." The Journal of Physical Chemistry B **124**(46): 10435-10441.
Skourtis, S. S., D. H. Waldeck and D. N. Beratan (2010). Fluctuations in Biological and Bioinspired Electron-Transfer Reactions. Annual Review of Physical Chemistry, Vol 61. S. R. Leone, P. S. Cremer, J. T. Groves, M. A. Johnson and G. Richmond. **61:** 461-485.
Šmídová, D., J. Lengyel, A. Pysanenko, J. Med, P. Slavíček and M. Fárník (2015). "Reactivity of Hydrated Electron in Finite Size System: Sodium Pickup on Mixed N2O–Water Nanoparticles." The Journal of Physical Chemistry Letters **6**(15): 2865-2869.
Smyth, M. and J. Kohanoff (2011). "Excess Electron Localization in Solvated DNA Bases." Physical Review Letters **106**(23): 238108.
Sprik, M., J. Hutter and M. Parrinello (1996). "Ab initio molecular dynamics simulation of liquid water: Comparison three gradient-corrected density functionals." Journal of Chemical Physics **105**(3): 1142-1152.
Suter, H. U. and T. Greber (2004). "On the dissociation of N2O after electron attaclnnent." Journal of Physical Chemistry B **108**(38): 14511-14517.
Takahashi, K., S. Ohgami, Y. Koyama, S. Sawamura, T. W. Marin, D. M. Bartels and C. D. Jonah (2004). "Reaction rates of the hydrated electron with N2O in high temperature water and potential surface of the N2O- anion." Chemical Physics Letters **383**(5-6): 445-450.
Todorova, T., P. H. Hünenberger and J. Hutter (2008). "Car–Parrinello Molecular Dynamics Simulations of CaCl2 Aqueous Solutions." Journal of Chemical Theory and Computation **4**(5): 779-789.
Troisi, A., M. A. Ratner and M. B. Zimmt (2004). "Dynamic Nature of the Intramolecular Electronic Coupling Mediated by a Solvent Molecule: A Computational Study." Journal of the American Chemical Society **126**(7): 2215-2224.
Troullier, N. and J. L. Martins (1991). "Efficient pseudopotentials for plane-wave calculations." Physical Review B **43**(3): 1993 LP - 2006.
Turi, L. and P. J. Rossky (2012). "Theoretical Studies of Spectroscopy and Dynamics of Hydrated Electrons." Chemical Reviews **112**(11): 5641-5674.
VandeVondele, J. and M. Sprik (2005). "A molecular dynamics study of the hydroxyl radical in solution applying self-interaction-corrected density functional methods." Physical Chemistry Chemical Physics **7**(7): 1363-1367.
Vchirawongkwin, V., H. Sato and S. Sakaki "RISM-SCF-SEDD Study on the Symmetry Breaking of Carbonate and Nitrate Anions in Aqueous Solution." The Journal of Physical Chemistry B **114**(32): 10513-10519.
Wu, X., L. Gao, J. Liu, H. Yang, S. Wang and Y. Bu (2015). "Excess electron reactivity in amino acid aqueous solution revealed by ab initio molecular dynamics simulation: anion-centered localization and anion-relayed electron transfer dissociation." Physical Chemistry Chemical Physics **17**(40): 26854-26863.